

# Module 3602: Surface Winds

Dr. Susanne Lehner, Dr. Andrey Pleskachevsky

Dr. Xiao-Ming Li, Dr. Stephan Brusch

Miguel Bruck, Domenico Velotto

German Aerospace Center (DLR)  
Remote Sensing Technology Institute  
SAR Signal Processing



# Content of Module Oceanography (3600)

- **3601: Oceanography Introduction**
- **3602: Surface wind**
  - Wind impact on sea surface
  - Empirical geophysical model functions
  - SAR wind inversions
  - SAR wind applications
- **3603: Ocean surface waves**
  - Ocean surface waves: physical background
  - SAR ocean surface wave imaging mechanism
  - SAR ocean wave inversions
  - Examples of sea state measurements
- **3604: Surface ocean currents**
  - Direct measurement of surface currents
  - Indirect measurement of surface currents
- **3605: Oil detection**
  - Oil imaging in SAR
  - Oil spill detection
  - Differences of oil and oil-like structures in SAR imagery

# Educational Objectives

- To get introduced to applications of SAR oceanography
- To get introduced to geophysical background
- To learn methods application possibilities, limitations and
- To learn the results applicability

# Requirements

- You know the basic concept of complex SAR data  
(Module ID 1101: Mathematics)
- You know and understand physical basics  
(Module ID 1104: Physics)
- You know and understand SAR technology  
(Module ID 1301: SAR Basics)

# Further Reading

- Alpers, W., Pahl, U., & Gross, G. (1998). Katabatic wind fields in coastal areas studied by ERS-1 synthetic aperture radar imagery and numerical modeling. *Journal Geophysical Research*, *103*, 7875–7886.
- Beal, R. C., Young, G. S., Monaldo, F., Thompson, D. R., N. S. Winstead, N. S., & Scott, C. A. (Eds.) (2005). *High resolution wind monitoring with wide swath SAR: A User's Guide*. Washington D.C.: U.S. Department of Commerce.
- Christiansen, M. B., & Hasager, C. B. (2005). Wake effects of large offshore wind farms identified from satellite SAR. *Remote Sensing of Environment*, *98*, 251-268.
- Hasager, C. B., Badger, M., Peña, A., Larsén, X. G., & Bingöl, F. (2011). SAR-based wind resource statistics in the Baltic Sea. *Remote Sensing*, *3*(1), 117-144.
- Johannessen, J. A., Shuchman, R. A., Johannessen, O. M., Davidson, K. L., & D. R. Lyzenga, D. R. (1991). Synthetic aperture radar imaging of upper ocean circulation features and wind fronts. *Journal of Geophysical Research*, *96*(C6), 10411–10422.
- Levy, G. (2001). Boundary layer roll statistics from SAR. *Geophysical Research Letter*, *28*, 1993– 1995.
- Monaldo, F., & Beal., R. (2004). Wind Speed and Direction. In C. R. Jackson, & J. R. Apel (Eds.), *Synthetic Aperture Radar (SAR) Marine User's Manual* (pp. 305-321). Washington DC: NOAA NESDIS Office of Research and Applications.
- Monaldo, F.M., Thompson, D. R., Pichel, W. G, & Clemente-Colón, P. (2004). A Systematic Comparison of QuikSCAT and SAR Ocean Surface Wind Speeds. *IEEE Transaction on Geoscience and Remote Sensing*, *42*(2), 283 - 291.

# 3602: Surface Wind

Wind impact on sea surface  
Empirical geophysical model functions  
SAR wind inversions  
SAR wind applications

Horns Rev. @David JC MacKay

# Applications of SAR Winds: different SAR sensors

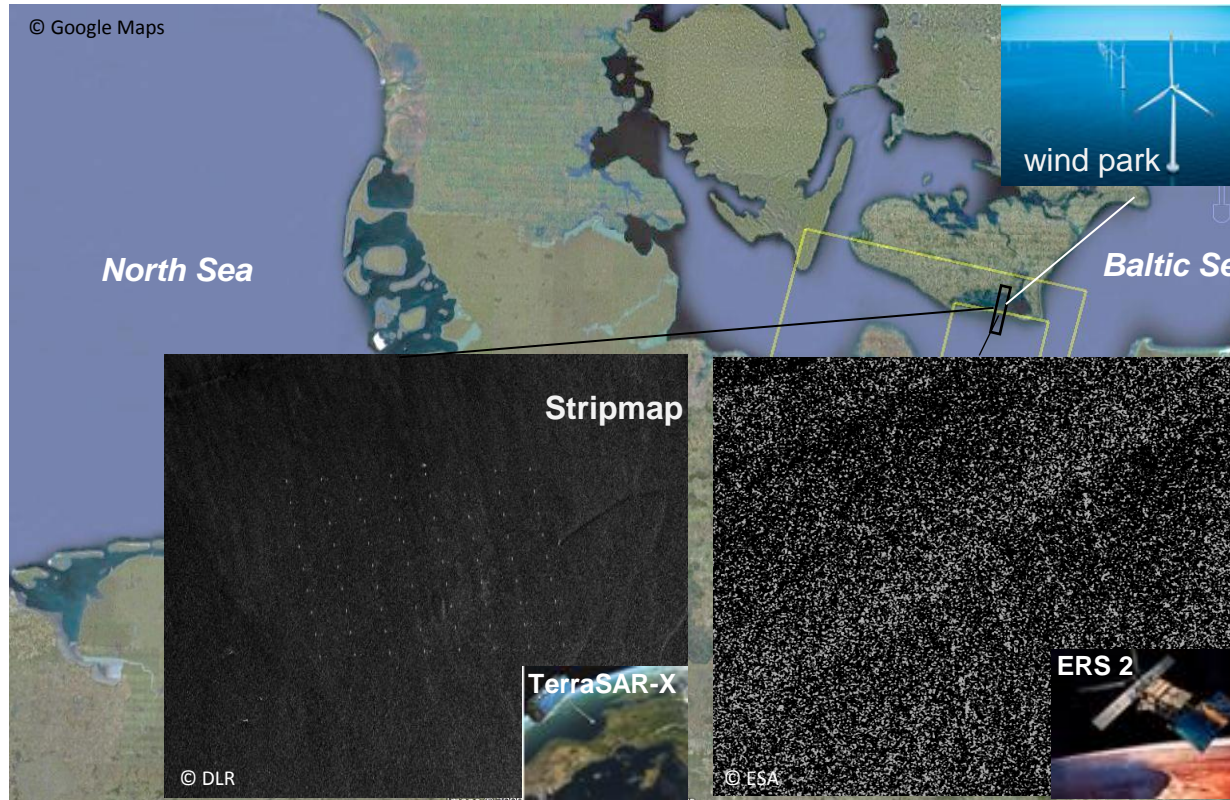
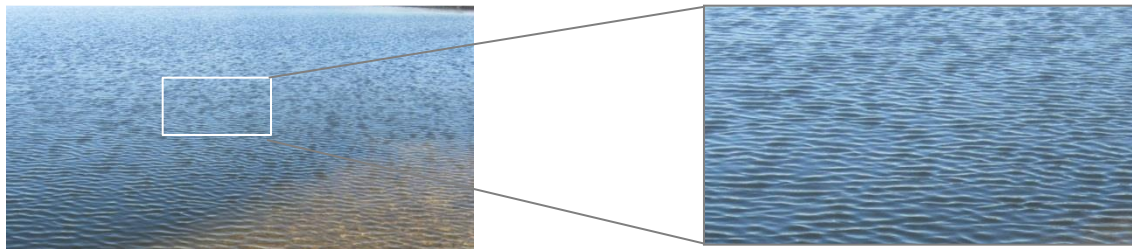


Fig. 6: High resolution SAR data show highly detailed spatial variability at ocean surface (© DLR). Due to its high spatial resolution, the SAR retrieved sea surface wind field is particularly used for coastal monitoring, to improve and assimilate into weather predictions, to monitor tropical and extra-tropical cyclones, to map katabatic and gap winds, to investigate atmospheric vortex streets and boundary layer rolls, as well as in support of offshore wind farming (see references). The following is focused on using TerraSAR-X and Tandem-X high spatial resolution data to monitor coastal wind field. The figure illuminates improvement of spatial resolution of TerraSAR-X (3 m for Stripmap in this case) compared to the previous ERS-2 SAR data (25 m). The bright points on the TerraSAR-X image are the offshore wind turbines over the Baltic Sea.

# Wind impact on sea surface: Physical background

Synthetic aperture radar is capable of providing wind information over the ocean by measuring the **roughness of the sea surface**.

stronger wind → surface roughness → stronger radar backscatter



**Capillary waves** traveling along the boundary layer of a fluid are dominated by the effects of surface tension. The source is the turbulent fluctuations of wind vector.

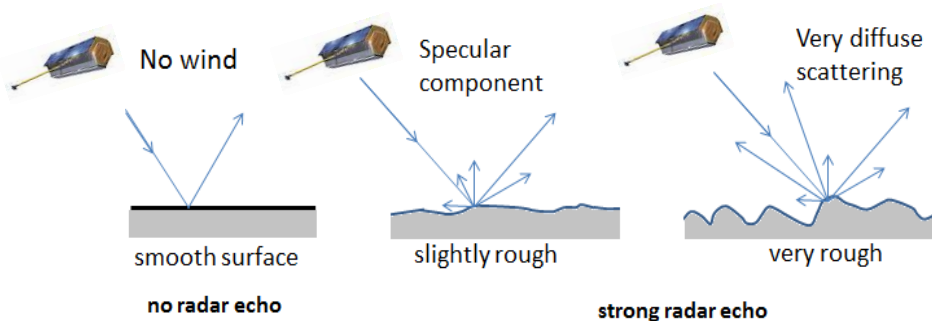


Fig. 7: SAR imaging of sea surface: capillary waves by wind (© DLR, Pleskachevsky)

# Wind direction from wind streak structures in SAR images

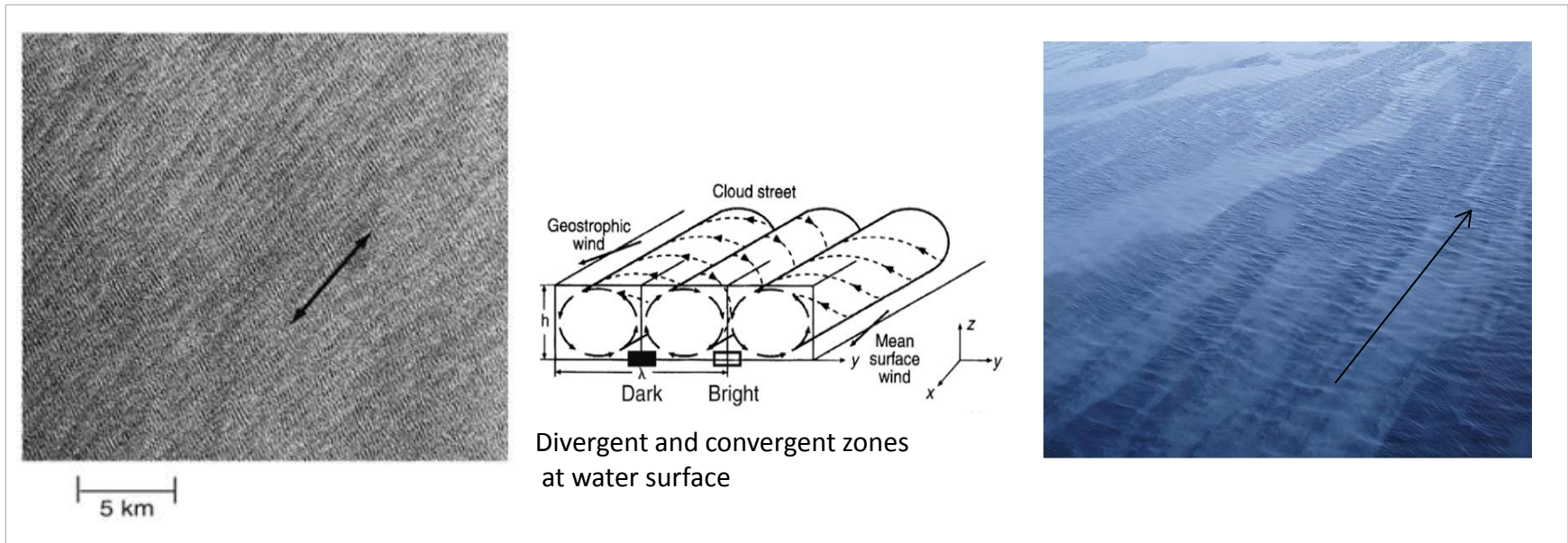


Fig. 8: Streak wind structures in SAR images: Streak structure are visible in radar images (as well in optical images). Up to today, the source of the wind-induced streaks visible in radar and optical images are under discussion. The major conclusion is that this linear streak features are induced by the Langmuir circulation. An area of downward flow causes more surface roughness and therefore brighter backscatter than an area of upward flow, thus creating a periodic structure in a SAR image. This wind streaks visible in SAR image is considered to be aligned with the direction of wind on the scale of a few kilometers in SAR imagery. Based on this rationale, the wind direction is estimated with an 180 directional ambiguity (© DLR, S. Brusch) (Extension ref. Gerling, 1986)

# Empirical Geophysical Model Functions (GMF)

Geophysical Model Function (GMF) empirically relates the Radar (e.g., Scatterometer and SAR) Normalized Radar Cross Section (NRCS,  $\sigma_0$ ) and incidence angle ( $\theta$ ) to the sea surface wind vectors (wind direction  $\varphi$  and speed  $v$ ). GMFs are generally described as:

$$\sigma_0 = B_0(v, \theta) (1 + B_1(v, \theta) \cos \phi + B_2(v, \theta) \cos 2\phi)$$

in which, relative wind direction  $\phi$  is defined as the angle between wind direction  $\varphi$  and radar looking direction  $\alpha$ , i.e.  $\phi = \varphi - \alpha$ .

The  $\sigma_0$  is largest if the wind blows toward to the radar look direction and is smallest when the wind blows perpendicularly.

An overview of some empirical GMFs for co-polarized and cross-polarized SAR data are given in following.

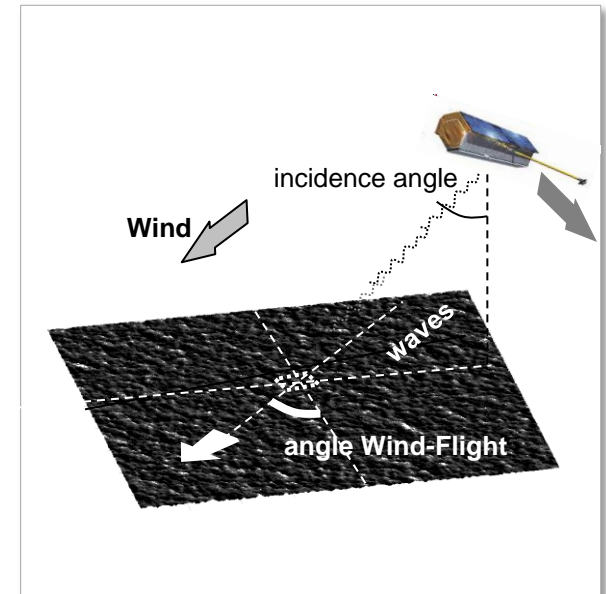


Fig. 9: Schema for surface wind estimation from SAR data (© DLR, Pleskachevsky)

# Empirical Geophysical Model Function (GMF)

## C-band GMF for Co-Polarized SAR (VV)

The GMF, called CMOD (C-band MODel) was originally developed by ESA for the C-band scatterometer onboard ERS-Satellites (ERS-1/2, <http://www.esa.int/esaEO/>). The widely used CMOD functions are the CMOD4 (Stoffelen *et al.*, 1997; Stoffelen, 1998) and CMOD 5 (Hersbach *et al.*, 2007), as well as its updated version CMOD5.N (Verhoef, *et al.*, 2008) to provide 10 m winds at neutral conditions. CMOD5 is developed particularly to improve performance for higher wind speeds. Another GMF (CMOD\_IFR2 (Quilfen *et al.*, 1998)) was developed independently at Ifremer, also with particular focus on retrieving higher wind speed.

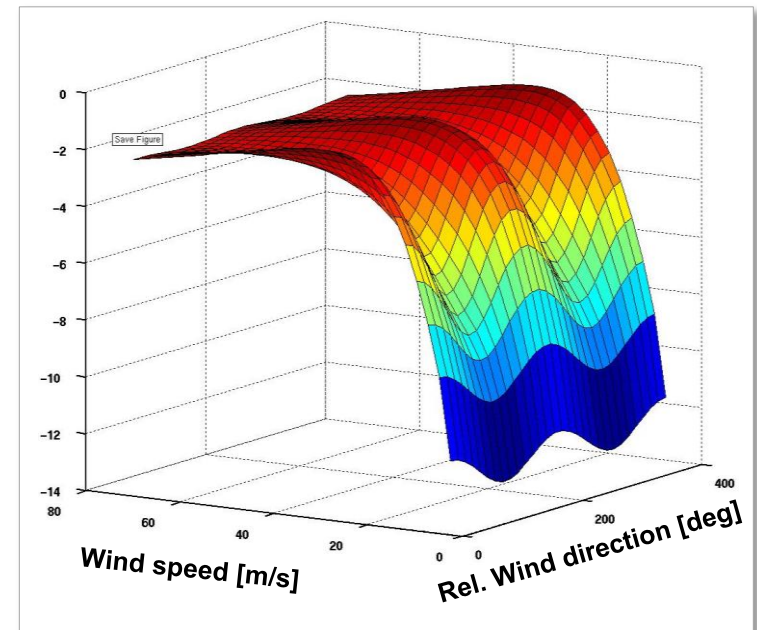


Fig. 10: Simulation of CMOD5 (© DLR, S. Lehner)

The left figure shows the dependence of  $\sigma_0$  with the sea surface wind speed and (relative) direction for incidence angle of  $30^\circ$ . The CMOD GMFs are also applicable to spaceborne **C-band SAR (e.g., the ERS-1/2 and ENVISAT/ASAR** data acquired in VV polarizations.

# Empirical Geophysical Model Function (GMF)

## C-band GMF for Co-Polarized SAR (HH)

The CMOD functions are applicable for radar NRCS acquired in VV polarizations. To apply the CMOD functions for NRCS in HH polarizations, **conversion of the  $\sigma_0^{HH}$  to  $\sigma_0^{VV}$  using the empirical Polarization Ratio (PR) Model** priori to apply the CMOD GMF is often considered.

**a) Three PR models which consider influence of the incidence angle on PR are often used.**

**Thompson model**

$$PR = \frac{\sigma_{VV}^0}{\sigma_{HH}^0} = \frac{(1 + 2 \tan^2 \theta)^2}{(1 + \alpha \tan^2 \theta)^2}$$

in which,  $\theta$  is incidence angle. Thompson *et al.* (1998) proposed  $\alpha=0.6$ . Both Vachon and Dobson (2000) and Horstmann *et al.* (2000) concluded that  $\alpha=1$  is suitable for the C-band RADARSAT-1 data.

**Elfouhaily model**

$$PR = \frac{\sigma_{VV}^0}{\sigma_{HH}^0} = \frac{(1 + 2 \tan^2 \theta)^2}{(1 + \beta \sin^2 \theta)^2}$$

$\beta = 2$  as proposed in [Elfouhaily and Thompson 1999]

**Mouche model**

$$PR = \frac{\sigma_{VV}^0}{\sigma_{HH}^0} = C_0 \text{EXP}(C_1 \theta) + C_2$$

$C_0 = 0.0065, C_1 = 0.1289, C_2 = 0.9928$  as proposed in [Mouche *et al.*, 2005]

**b) In addition, influence of wind speed and sea state on PR are also considered (Mouche *et al.*, 2005; Zhang *et al.*, 2011).**

# Empirical Geophysical Model Function (GMF)

## C-band GMF for Cross-Polarized SAR (VH, HV)

Unlike the NRCS in co-polarization SAR has a nonlinear dependence on wind direction and incidence angle in addition to wind speed, the cross-polarized SAR NRCS is shown has only dependence on wind speed (Vachon and Wolfe, 2011; Zhang *et al.*, 2011). Thus, wind speed can be retrieved from cross-polarized SAR images directly without the need for external wind direction information, which in fact is the case for co-polarized SAR images. However, as the NRCS in the cross-polarized SAR data is much lower than that in the co-polarized data, there are some limitations for retrieving the sea surface wind speed below 10 m/s.

For cross-polarized SAR data, the GMF called C-2PO (C-band Cross-Polarized Ocean) Model is developed [Zhang *et al.*, 2011] using the RADARSAT-2 Quad-polarization data, which exhibits a distinctly linear relationship between the NRCS and wind speed. The C-2PO model relates the cross-pol NRCS to wind speed at 10 m height ( $U_{10}$ ) according to:

$$\sigma_{VH}^o = 0.580 * U_{10} - 35.652$$

In which, the units of  $\sigma_0^{VH}$  and  $U_{10}$  are dB and m/s, respectively. An example of this relation is shown in the right panel. It should be noted that radar returns in cross-polarized data are generally much weaker than that in co-polarized data, implying that the accuracy of radiometric calibration is therefore of vital importance.

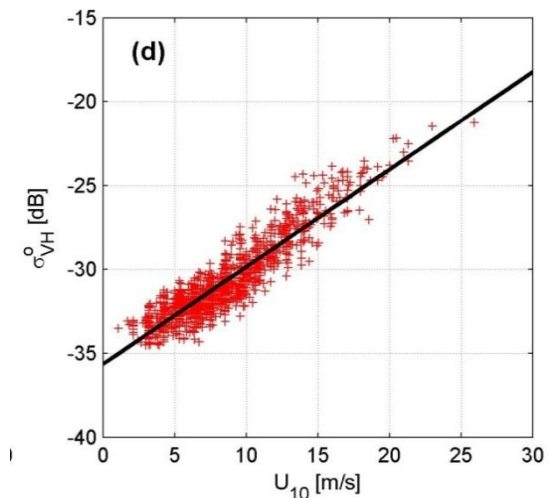


Fig.11: (Courtesy by B. Zhang at BIO, Canada)

# Empirical Geophysical Model Function (GMF)

## L-band GMF for JERS-1 SAR and ALOS-PALSAR (HH polarization)

Wind features were in fact clearly visible in early L-band SAR images from SEASAT, which was launched in 1978 and operated for only 105 days. Two L-band SAR sensors, i.e., the JERS-1 (1992) and the ALOS-PALSAR (2006) have later been launched by the Japan Aerospace Exploration Agency (JAXA). The L-band GMF was developed by Shimada *et al.* (2003) for JERS-1 SAR data and its updated version (Isoguchi and Shimada, 2009) for the PALSAR data. Both GMFs are tuned by collocating SAR NRCS to scatterometer wind vectors.

The L-band and HH polarized SAR onboard JERS-1 featured a high resolution of 18 m, a fixed off-nadir angle of 35°. It is found that influence of incidence angle on NRCS within 37° to 42° is negligible. Thus, a L-band GMF for JERS-1 is based on a linear combination of functions of wind speed and direction. Here,  $\phi$  is relative wind direction. Coefficients  $a_0, a_1, a_2,$  and  $a_3$  are functions of wind speed. Detailed of these functions are available in [Shimada *et al.*, 2003].

$$\sigma_0^{lin} = a_0 + a_1 \cos \phi + a_2 \cos 2\phi + a_3 \cos 3\phi$$

The L-band GMF for PALSAR data has the same expression as the CMOD functions, i.e.,

$$\sigma_0 = B_0(v, \theta) (1 + B_1(v, \theta) \cos \phi + B_2(v, \theta) \cos 2\phi)$$

However, the transfer functions in the three terms of  $B_0$ ,  $B_1$  and  $B_2$  in the L-band GMF are different from those used in CMOD4 or CMOD5. The detailed descriptions are available at [Isoguchi and Shimada, 2009]. Due to the longer radar wavelength (23.6 cm for PALSAR), the L-band wind sensitivity is less than the C-band one at large incidence angles and moderate winds.

# Empirical Geophysical Model Function (GMF)

## X-band GMF for TerraSAR-X and Tandem-X (VV and HH polarization)

- ✓ The **XMOD1** (Ren *et al.*, 2012) was first developed to relate empirically the X-band SAR NRCS to the sea surface wind vectors. It has the function as:

$$\sigma_o = x_0 + x_1 v + x_2 \sin(\theta) + x_3 \cos(2\phi) + x_4 v \cos(2\phi)$$

$x_0$ ,  $x_1$ ,  $x_2$  and  $x_3$  are coefficients tuned by collocating SIR-X NRCS to the ECMWF numerical model results.  $\theta$  is incidence angle in unit of degree and  $\phi$  is relative wind direction, and  $v$  is sea surface wind speed at 10 m height.

- ✓ The newly developed **XMOD2** [Li and Lehner, 2012] is a non-linear GMF, which has the same general expression as CMOD5, i.e.,

$$\sigma_o = B_0^p(v, \theta) (1 + B_1(v, \theta) \cos \phi + B_2(v, \theta) \cos 2\phi)$$

# Empirical Geophysical Model Function (GMF)

X-band GMF for TerraSAR-X and Tandem-X (VV and HH polarization)

Comparisons between XMOD1 and XMOD2 under different conditions.

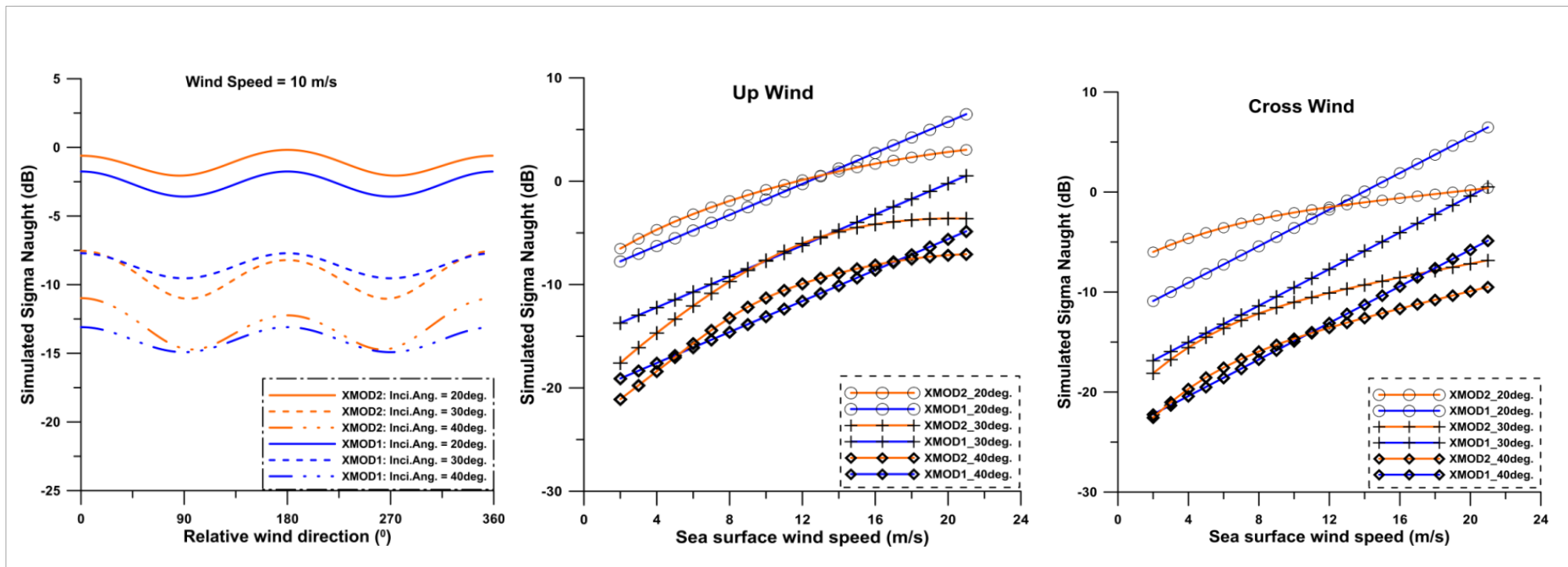


Fig. 12: Simulation of XMOD1 and XMOD2 GMF (Courtesy by X.-M. Li at DLR)

# Empirical Geophysical Model Function (GMF)

- ✓ To apply the XMOD1 and XMOD2 for TerraSAR-X and Tandem-X data acquired at HH polarization, two Polarization Ratio model are developed [Shao *et al.*, 2012]. One is based on the retuning of the Elfouhaily PR model using TerraSAR-X data acquired in dual-polarization mode.  $\beta$  is 2.47 in the following function.

**Elfouhaily-X model**

$$PR = \frac{\sigma_{VV}^0}{\sigma_{HH}^0} = \frac{(1 + 2 \tan^2 \theta)^2}{(1 + \beta \sin^2 \theta)^2}$$

The other one is based on the empirical function given in [Masuko *et al.*, 1986], with retuned coefficients of  $X_0 = 0.61$  and  $X_1 = 0.02$  in the following function.

**X-PR model**

$$PR = \frac{\sigma_{VV}^0}{\sigma_{HH}^0} = X_0 \text{EXP}(X_1 \theta)$$

- ✓ In addition to develop a detailed GMF to relate X-band NRCS to the sea surface wind vectors, Thompson *et al.* (2012) applied a different approach to develop an X-band GMF by interpolating the coefficients of well-tested C-band and Ku-band GMFs.

# Empirical Geophysical Model Function (GMF)

## Doppler shift GMF for Co-Polarized C-band SAR (VV, HH)

In addition to develop an empirical GMF to relate SAR NRCS to the sea surface wind vectors, the „Doppler Shift“ methodology is the other approach to estimate the sea surface wind speed. The „CDOP“ GMF was developed by (Mouche *et al.*, 2012) by collocating the Doppler anomalies measured in ASAR data with the ASCAT scatterometer wind vectors. The CDOP GMF was developed for both HH- and VV- polarizations. An example showing the dependence of the Doppler Centroid anomaly on wind direction under wind speed of 7m/s is giving below. It is showed in Mouche *et al.* (2012) how the combination of NRCS and Doppler helps to better constrain the wind inversion and improve the wind direction retrieval (particularly interesting in cases of front, low pressure system etc...).

It is necessary to point out that the Doppler shift also contains contributions from the radial ocean surface currents and waves. Thus, unless the current is negligible or directly along the azimuth direction, this component should be subtracted priori to retrieval of sea surface wind.

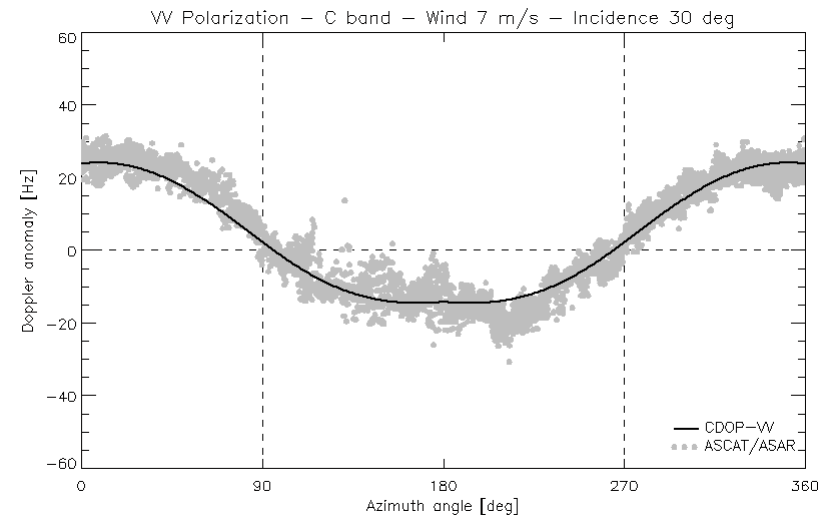


Fig. 13: Envisat ASAR Doppler Centroid anomaly for VV polarization against relative wind direction for wind speed of 7 m/s and incidence angle of 30° (Courtesy by A. Mouche from CLS)

# SAR wind inversions

The GMFs introduced previously indicates that radar NRCS relates to both the sea surface wind speed and direction. Scatterometer has multiple beams, which ensures to obtain both wind direction and speed simultaneously. However, SAR systems have only one antenna. To retrieve the sea surface wind field from high spatial resolution SAR data, the wind direction needs to be determined primarily. There are generally two methodologies are available to retrieve the sea surface wind direction from SAR imagery.

- **FFT method.** It is introduced previously that the wind streaks in SAR imagery are align with sea surface wind direction. Therefore, where wind streaks are visible, they can be used to estimate the wind direction up to  $180^\circ$  ambiguity, finding the dominant direction faster Fourier Transform (FFT) (e.g., described in Gerling, 1986)
- **Local-Gradient (LG) Method.** Different with the FFT method conducted in the spectral domain, the LG method is applied in the spatial domain while it also depends on visible wind streaks in SAR image. The ideal wind streak is about constant along its direction and strongest varying about orthogonal to its direction. As the direction of strongest increase is given by the gradient, the direction of a wind streak is about orthogonal to the gradient direction. Thus the wind direction, which is considered to be align with wind streaks, also perpendicular to the direction of the gradient. (Koch, 2004; Horstmann and Koch, 2005)

comment

The  $180^\circ$  ambiguity of the estimated wind direction using FFT method or LG method can be removed depending on spatial variations of the sea surface wind field, particularly, over coastal zones where topography/orography often has significant effect on sea surface wind field. (Extension ref. Lehner *et al.*, 1998; Horstmann *et al.*, 2000, etc.). Where the wind streaks are not visible in SAR image, the Projection method (Wackermann *et al.*, 2003) is applied to estimate wind direction. Alternatively, forecast of numerical models, such as ECMWF, NCEP GFS or WRF, are often used as a priori to estimate sea surface wind direction from SAR image. This works generally well where wind direction gradients are smooth, but less satisfactory near strong wind direction gradients, such as fronts and cyclones. Taking wind directions from scatterometer measurements can work better if such measurements are available close to SAR acquisitions, ideally less than one hour.

# Workflow to retrieve sea surface wind from SAR

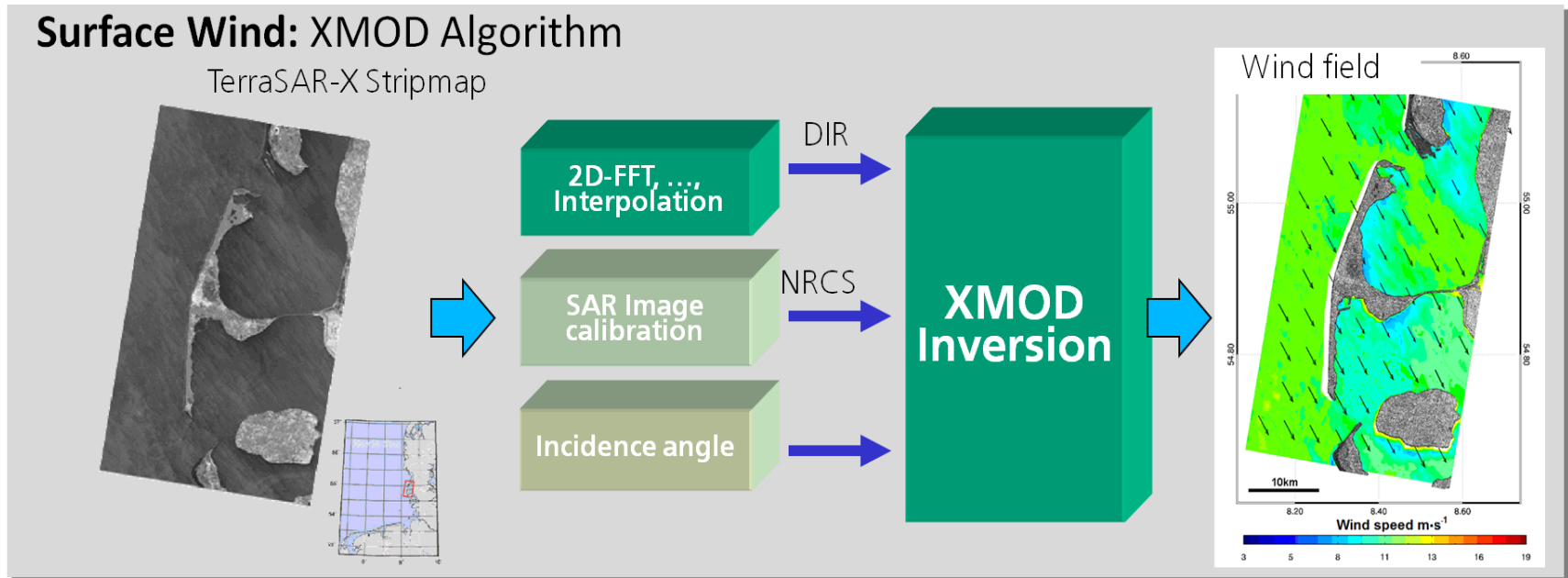


Fig. 14: Workflow for wind field estimation from SAR data (© DLR, Brusch)

In fact, size of the SAR subscene used to estimate sea surface wind direction should be larger than 10 km, as typical scale of wind streaks varies between 2 km and up to 10 km under different wind situations. Therefore, to retrieve sea surface wind field from SAR in high spatial resolution in scale of kilometer, interpolation technique should be considered (Reppucci *et al.*, 2010). After the sea surface wind direction is available, the sea surface wind speed can be retrieved using the GMFs described previously.

# TerraSAR-X and Tandem-X wind field: examples

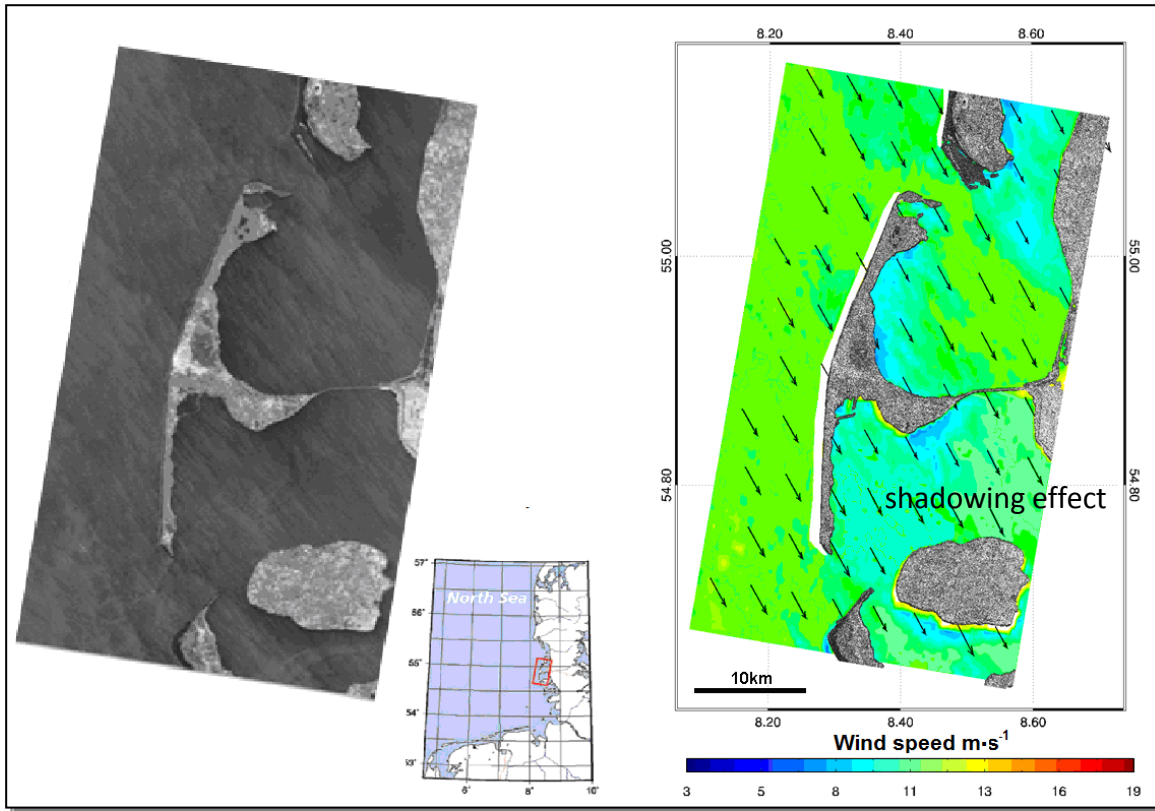


Fig. 15: Wind speed retrieved from HH polarized Stripmap data of TerraSAR-X acquired over Sylt Island, North Sea on March 26, 2008 and XMOD derived wind field (wind speed errors due to insufficient information are masked by white colour) (Lehner et al, 2012).

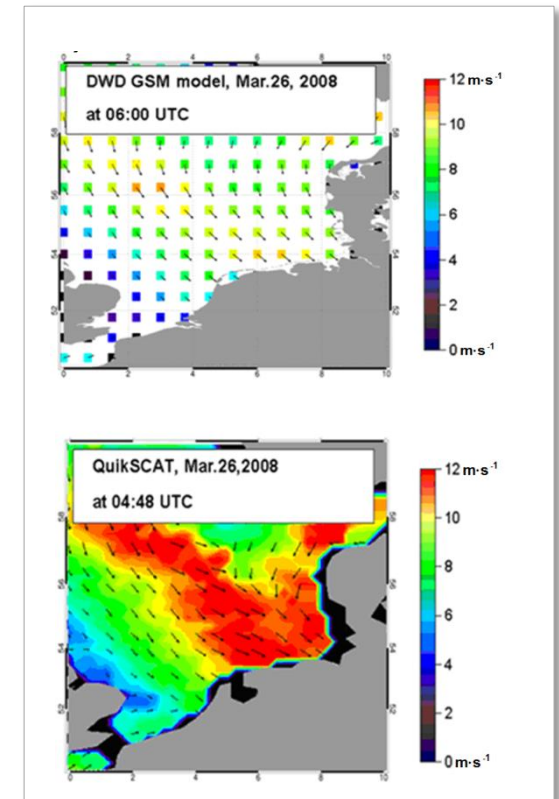


Fig.16: Wind from QuikSCAT scatterometer data (25km resolution) and the DWD forecast model GSM ( $0.75^\circ$  res.) for the North Sea. The retrieved TS-X wind fields show fine-scale turbulence effects which are not visible in coarser model, SAR and SCAT data) (Lehner et al, 2012).

# Wind field from SAR data: *Alpha Ventus* Wind Park



Fig. 17: Wind estimation from TerraSAR-X Stripmap image for *Alpha Ventus* Offshore Wind Park in the North Sea (© DLR, Li)

# Wind field from SAR data: *Alpha Ventus* Wind Park

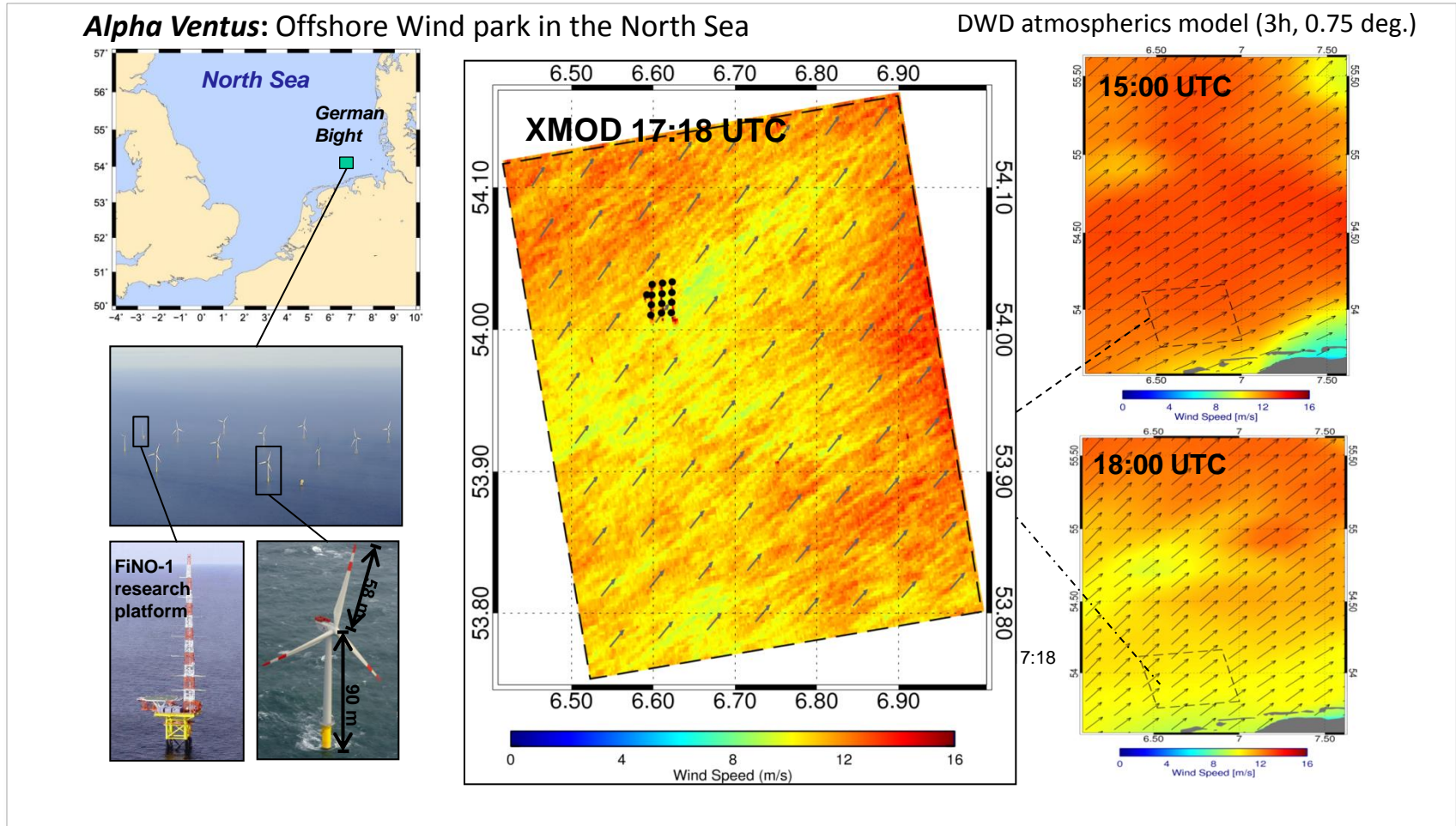


Fig. 18: Wind estimation from TerraSAR-X Stripmap image for *Alpha Ventus* Offshore Wind Park in the North Sea. Comparison to DWD model (© DLR)

# Wind field from SAR data: *Alpha Ventus* Wind Park

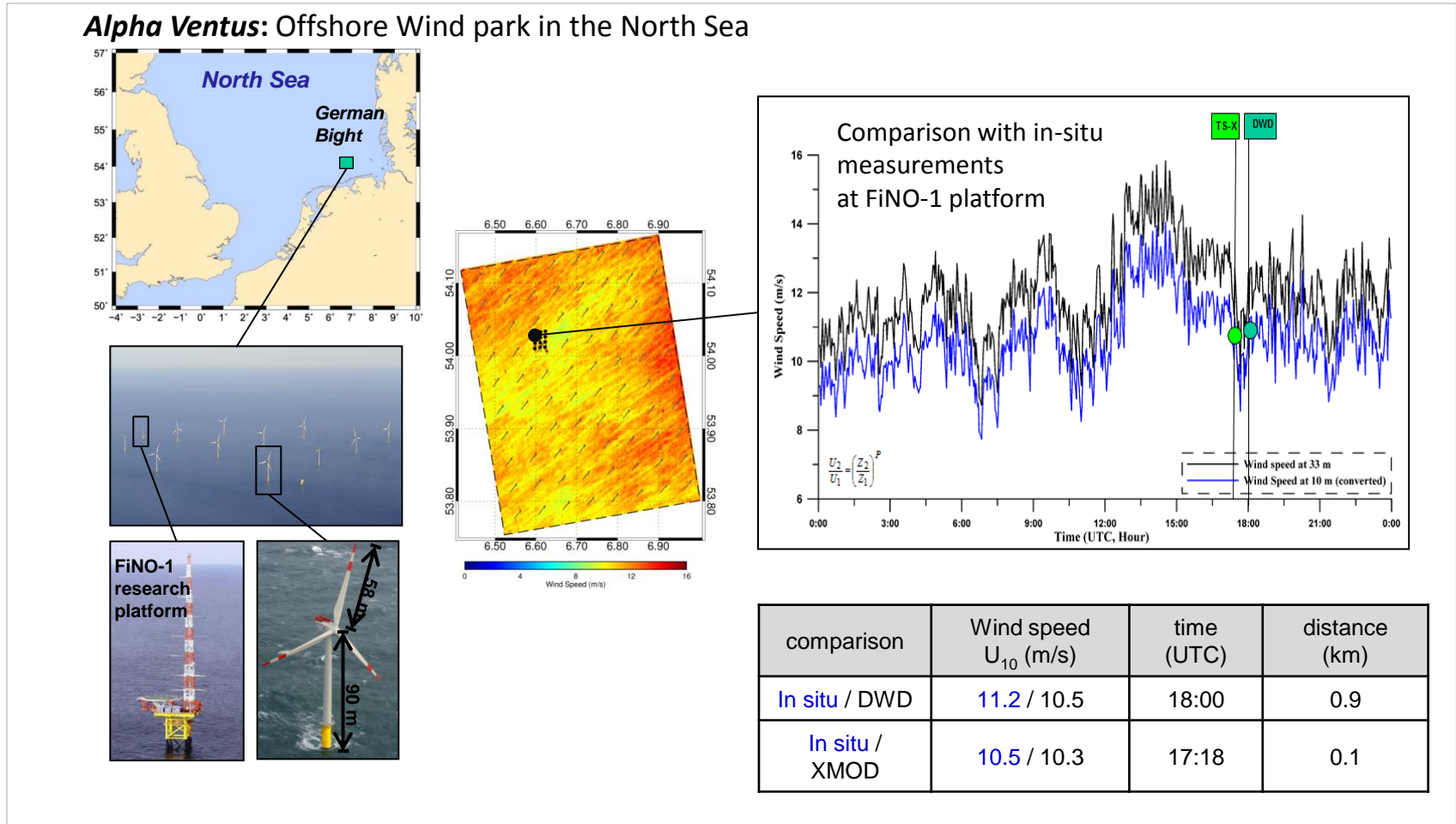


Fig. 19: Wind estimation from TerraSAR-X Stripmap image for *Alpha Ventus* Offshore Wind Park in the North Sea. Comparison to in-situ measurements (© DLR)

# Wind field from SAR data: *Typhoon*

XMOD

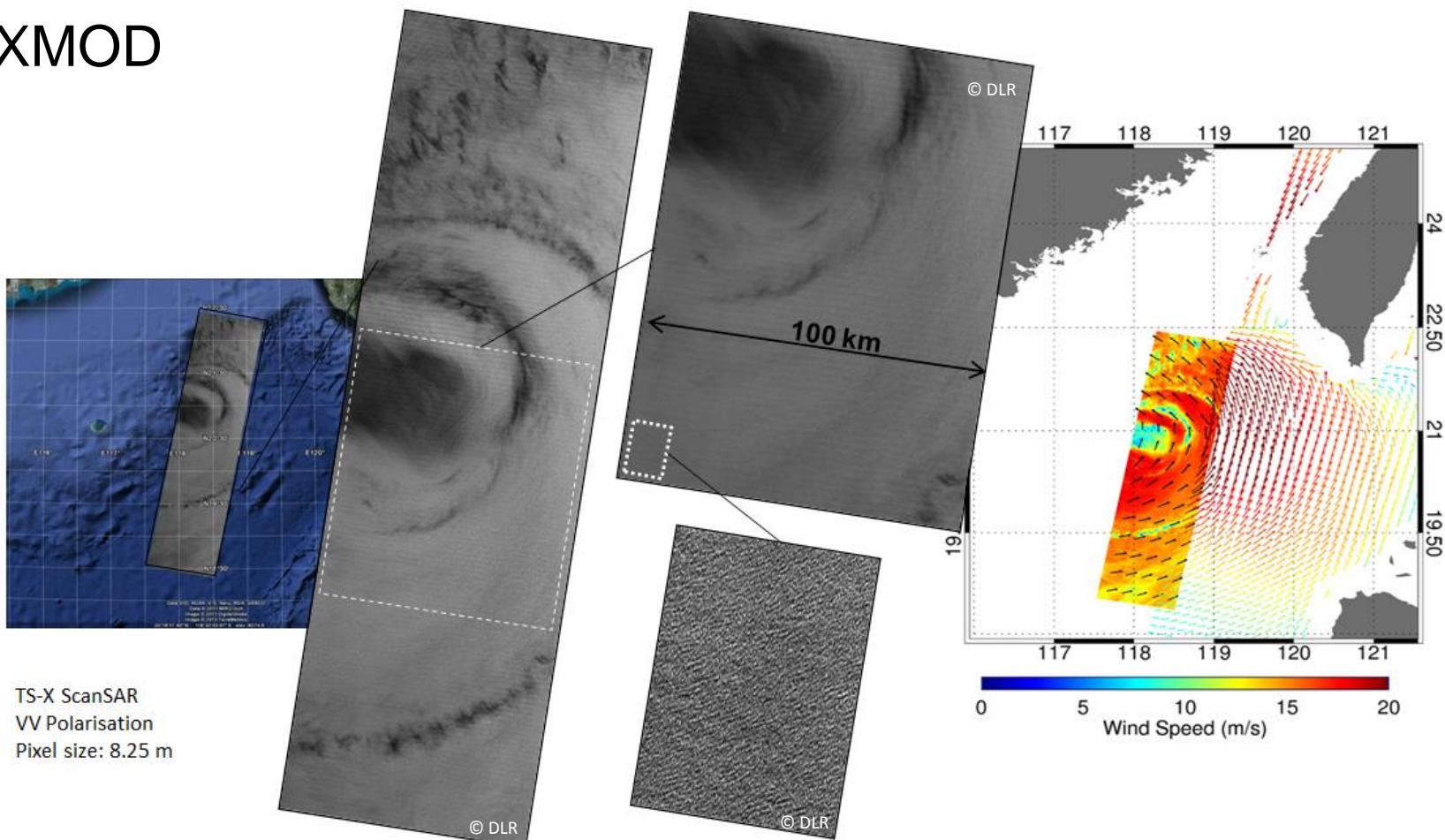


Fig. 20: Tropical Cyclone Eye “MEGI” SSW measurement of Typhoon using TSX-SC data (© DLR)

# Wind field from SAR data: *Hurricanes*

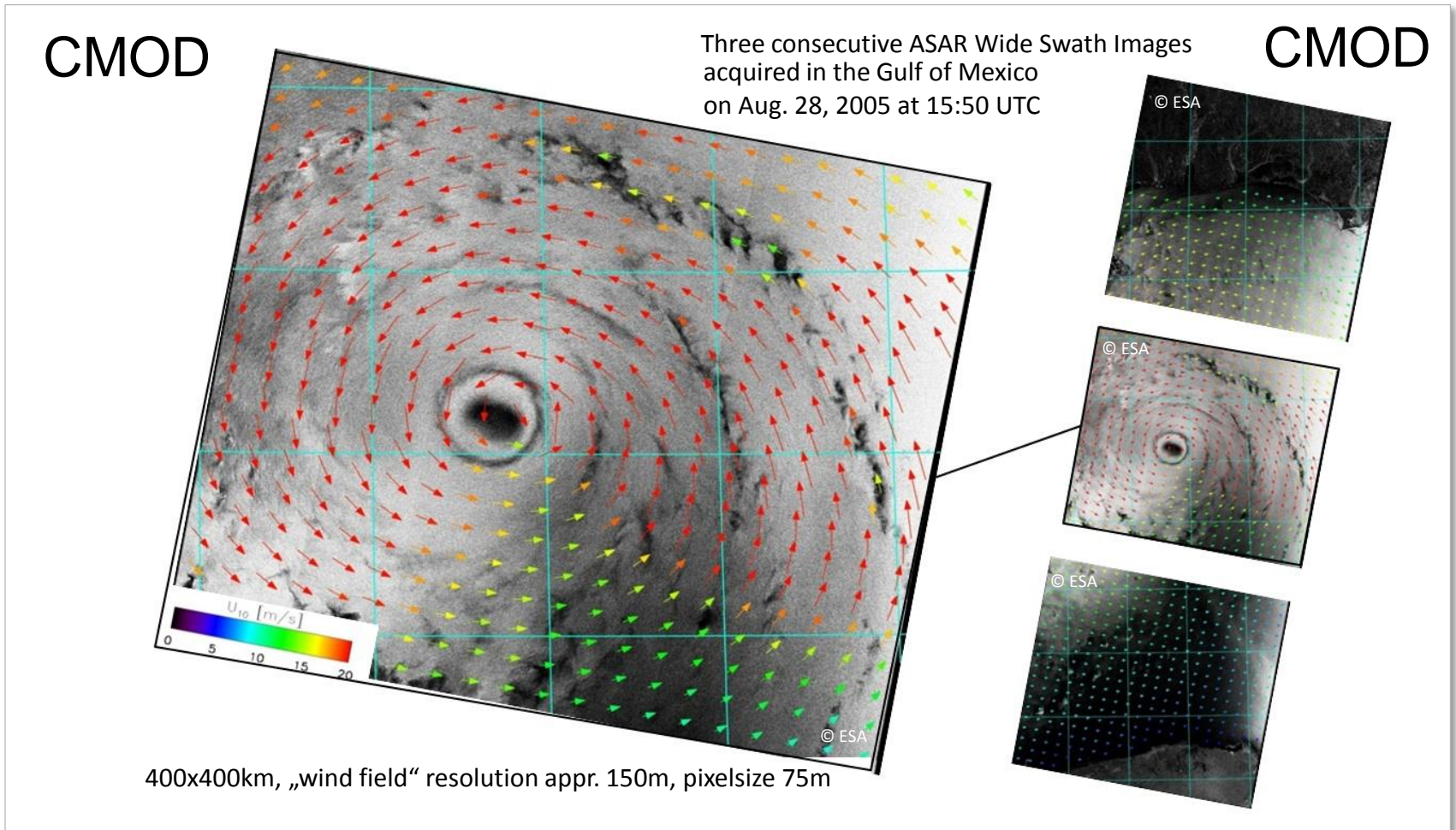


Fig. 21: SAR sea surface wind field for tropical cyclones: Hurricane Katrina, August, 2005 (© DLR, Lehner)

# References: sea surface wind from SAR (1)

- Gerling, T. W. (1986). Structure of the surface wind field from the Seasat SAR. *Journal of Geophysical Research*, *91*, 2308-2320.
- Hersbach, H., Stoffelen, A., & de Haan, S. (2007). An improved C-band scatterometer ocean geophysical model function: CMOD5. *Journal of Geophysical Research*, *112*, C03006, doi:10.1029/2006JC003743.
- Horstmann, J., & Koch, W. (2005). Measurement of ocean surface winds using synthetic aperture radars. *IEEE Oceanic Engineering*, *30*(3), 508-515.
- Horstmann, J., Koch, W., Lehner, S., & Tonboe, R. (1999). Computation of wind vectors over the ocean using spaceborne synthetic aperture radar. *Johns Hopkins APL Technical Digest*, *21*(1), 100–107.
- Isoguchi, O., & Shimada, M. (2009). An L-band ocean geophysical model function derived from PALSAR. *IEEE Transactions on Geoscience and Remote Sensing*, *47*(7), 1925–1936.
- Lehner, S., Horstmann, J., Koch, W., & Rosenthal, W. (1998). Mesoscale wind measurements using recalibrated ERS SAR images. *Journal of Geophysical Research*, *103*(C4), 7847-7856.
- Lehner, S., Pleskachevsky, A., & M. Bruck (2012). High resolution satellite measurements of coastal wind field and sea state. *International Journal of Remote Sensing*, *33*(23), 7337-7360.
- Li, X.-F., Clemente-Colon, P., Pichel, W. G., & Vachon, P. W. (2000). Atmospheric vortex streets on a RADARSAT SAR image. *Geophysical Research Letter*, *27*, 1655–1658.
- Li, X.-F., Zheng, W., Pichel, W. G., Zou, C.-Z., & Clemente-Colón, P. (2007). Coastal katabatic winds imaged by SAR. *Geophysical Research Letter*, *34*(3), L03804, doi:10.1029/2006GL028055.

# References: sea surface wind from SAR (2)

- Mouche, A. A., Collard, F., Chapron, B., Dagestad, K.-F., Guitton, G., Johannessen, J. A., Kerbaol, V., & Hansen, M. W. (2012). On the use of Doppler shift for sea surface wind retrieval from SAR. *IEEE Transactions on Geoscience and Remote Sensing*, 50(7), 2901-2909.
- Mouche, A. A., Hauser, D., Daloze, J. F., & Guerin, C. (2005). Dual polarization measurements at C-Band over the ocean: Results from airborne radar observations and comparison with ENVISAT ASAR data. *IEEE Transaction on Geoscience and Remote Sensing*, 43, 753–769.
- Quilfen, Y., Chapron, B., Elfouhaily, T., Katsaros, K., & Tournadre, J. (1998). Observation of tropical cyclones by high-resolution scatterometry. *Journal of Geophysical Research*, 103(C4), 7767–7786, doi:10.1029/97JC01911.
- Ren, Y., Brusch, S., He, M., Lehner, S., & Li, X. (2012). An Algorithm for the Retrieval of Sea Surface Wind Fields using X-Band TerraSAR-X Data. *International Journal of Remote Sensing*, 33(23), 7310-7336.
- Reppucci, A., Lehner, S., Schulz-Stellenfleth, J., & Brusch, S. (2010). Tropical Cyclone Intensity Estimated from Wide Swath SAR Images. *IEEE Transactions on Geoscience and Remote Sensing*, 48 (4), 1639-1649.
- Shimada, T., Kawamura, H., & Shimada, M. (2003). An L-band geophysical model function for SAR wind retrieval using JERS-1 SAR. *IEEE Transactions on Geoscience and Remote Sensing*, 41(3), 518–531.
- Stoffelen, A. C. M. (1998). Error modeling and calibration; towards the true surface wind speed. *Journal of Geophysical Research*, 103(C4), 7755-7766.

# References: sea surface wind from SAR (3)

- Stoffelen, A. C. M., & Anderson, D. L. T. (1997). Scatterometer data interpretation: derivation of the transfer function CMOD4. *Journal of Geophysical Research*, 102(C3), 5767-5780.
- Thompson, D. R., Elfouhaily, T. M., & Chapron, B. (1998). Polarization ratio for microwave backscattering from the ocean surface at low to moderate incidence angles. In: *Proceedings of the International Geoscience and Remote Sensing Symposium (IGARSS)* (pp. 1671-1673), July 6 - 10, 1998, Seattle, USA.
- Vachon, P. W., & Wolfe, J. (2011). C-band cross-polarization wind speed retrieval. *IEEE Geoscience and Remote Sensing Letters*, 8, 456-459.
- Verhoef, A., Portabella, M., Stoffelen, A. C. M., & Hersbach, H. (2008). *CMOD5.n - the CMOD5 GMF for neutral winds*. Retrieved November, 11, 2012 from [http://www.knmi.nl/publications/fulltexts/cmod5\\_neutral\\_winds\\_1.0.pdf](http://www.knmi.nl/publications/fulltexts/cmod5_neutral_winds_1.0.pdf)
- Wackerman, C., Pichel, W. G., & Clement-Colón, P. (2003). A projection method for automatic estimation of wind vectors with RADARSAT SAR imagery. In: *Proceedings of the 2nd Workshop on Coastal and Marine Applications of SAR* (pp. 55-60), September 8 – 12, 2003, Svalbard, Norway.
- Zhang, B., Perrie, W., & HE, Y.-J. (2011). Wind speed retrieval from RADARSAT-2 quad-polarization images using a new polarization ratio model. *Journal of Geophysical Research*, 116(C8), doi: 10.1029/2010JC006522.



Dr. Susanne **Lehner**



Miguel **Bruck**



Domenico **Velotto**



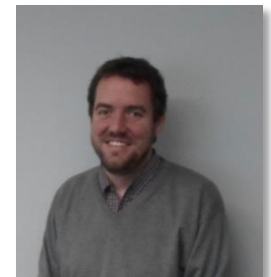
Dr. Thomas **König**



Dr. Xiao-Ming **Li**



Dr. Andrey  
**Pleskachevsky**



Dr. Stephan **Brusch**

# SAR-EDU – SAR Remote Sensing Educational Initiative

<https://saredu.dlr.de/>

Supported by:



Federal Ministry  
of Economics  
and Technology

on the basis of a decision  
by the German Bundestag